

Calculating spatiotemporally modulated surfaces: a dynamical differential formalism

Daigo Oue,¹ Kun Ding,^{1,2} and J. B. Pendry¹

¹*The Blackett Laboratory, Department of Physics, Imperial College London,
Prince Consort Road, Kensington, London SW7 2AZ, United Kingdom*

²*Department of Physics, State Key Laboratory of Surface Physics,
and Key Laboratory of Micro and Nano Photonic Structures
(Ministry of Education), Fudan University, Shanghai 200438, China*

(Dated: November 28, 2021)

Electromagnetic waves in a system with a space and time dependent boundary experience both diffraction and Doppler-like frequency conversion. In order to analyse such situations, conventional methods call for either the eigenmodes or the dyadic Green's function in space and time dependent media. Here, we propose a dynamical differential method which does not require either of them. Our method utilises a dynamical coordinate transformation in order to simplify the calculation of the optical response of the space and time dependent system. We reveal that the diffraction symmetry is broken in the presence of traveling-wave type spatiotemporal modulation.

I. INTRODUCTION

Recently, spatiotemporal modulation of bulky media has been studied both theoretically and experimentally [1–5]. The modulation breaks reciprocity in the media and brings about unique phenomena such as light amplification and the Fresnel drag. Keeping these in mind, in this work, we analyse the light scattering by spatiotemporally modulated surfaces.

One way to calculate the light scattering is to use the dyadic Green's function in the system in question. Once we obtain the dyadic Green's function in the system, we can perturbatively calculate the scattered field from incident field and thus the scattering matrix, [6, 7].

Another approach is the boundary matching method. In this approach, the incident and scattered fields are expanded in series of the eigenmodes in the system, and the field continuity conditions are imposed at the boundaries, which lead to simultaneous equations. The inversion of the equation system yields the scattering matrix. Calculation of the Mie coefficients [8] is one of the popular examples where boundary matching approach is taken.

Here, we consider the boundary matching at a dynamically deformed boundary with the help of a differential formalism. The differential formalism is originally proposed by Chandezon et al. to calculate dielectric gratings [9–11]. Since this method allows to directly match the boundary conditions at structured interfaces, the geometry is properly captured. One significance of the differential formalism is its convergence. When the formalism is numerically implemented, it shows steady convergence even in the presence of sharp edges [12, 13]. This is why it has been used to calculate not only dielectric gratings but also dispersive, lossy, anisotropic gratings [14–19]. In the current work, we extend the formalism to dynamical systems so that we can take the motion of the interface as well as the geometry.

There is a related approach based on conformal transformations proposed by Ward and Pendry [20], in which a surface structure is encoded into a conformal mappings.

This approach is also widely used in optics and plasmonics communities [21–26]. Compared to the conformal approach, the method utilised in this paper is more straightforward when it comes to analysing systems with time dependent boundaries because we can directly use time-dependent surface profile instead of finding corresponding conformal transformation.

This paper is organised as following. In Sec. II, we extend a differential formalism so as to enable the electromagnetic field analysis in the presence of a dynamically modulated boundary. In Sec. III, we numerically implement the dynamical differential formalism. We will also see the calculation is consistent with effective medium description. The conclusion is drawn in Sec. IV.

II. DYNAMICAL DIFFERENTIAL FORMALISM

As a simple example of the dynamically modulated surfaces, we consider a sinusoidally modulated boundary shown in FIG. 1.

The profile of the boundary is given by

$$a_{\mathbf{x}} = A \sin(\mathbf{q} \cdot \mathbf{x}) = A \sin \left[g \left(x - \frac{\Omega}{g} t \right) \right] \quad (1)$$

Here, we have introduced three-component vectors $\mathbf{q} = \{g, 0, -i\Omega/c\}$ and $\mathbf{x} = \{x, y, -ict\}$, where A , g and Ω are the strength of the modulation, the spatial and temporal frequencies of the modulation, respectively. The surface is not physically moving in the x direction, but its profile is shifting at the phase velocity Ω/g that can exceed the speed of light.

The permittivity distribution is given by means of the boundary profile,

$$\epsilon_{\mathbf{x},z} = \epsilon^< \Theta(a_{\mathbf{x}} - z) + \epsilon^> \Theta(z - a_{\mathbf{x}}) \quad (2)$$

$$= \alpha \Theta(a_{\mathbf{x}} - z) + \epsilon^>, \quad (3)$$

where Θ represents the Heaviside unit step function, and $\alpha \equiv (\epsilon^< - \epsilon^>)$ corresponds to the permittivity difference.

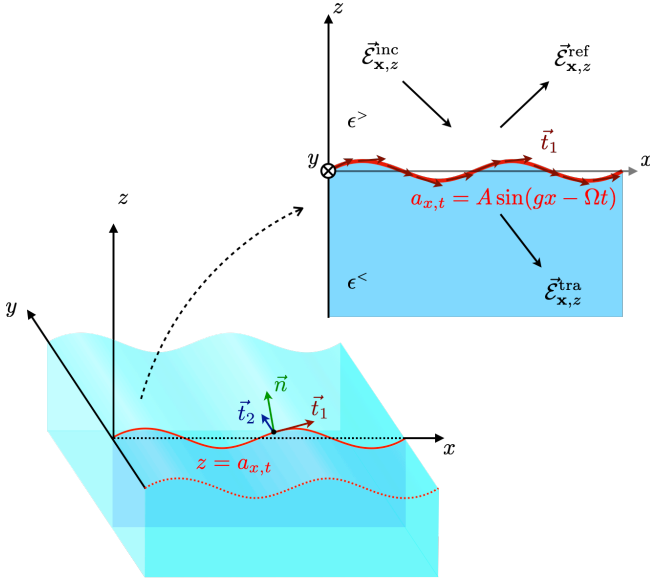


FIG. 1. Spatiotemporally modulated surface. The surface is weakly modulated in space and time. The corrugation function is sinusoidal and given by Eq. (1). We consider in-plane incidence of electromagnetic field and analyse the reflection and the transmission at the surface. The red and blue arrows $\vec{t}_{1,2}$ are the tangential vectors of the surface at each point. The permittivities of medium and lower media are ϵ^{\lessgtr} , respectively. The permeability is assumed to be unity in both media, $\mu^{\lessgtr} = 1$.

We can calculate tangential and normal vectors of the surface, $\vec{t}_{1,2}$ and \vec{n} , by taking the partial derivatives of the boundary profile (1),

$$\begin{cases} \vec{t}_1 = \frac{\vec{u}_x + a'_x \vec{u}_z}{\sqrt{1 + a'^2_x}}, & \vec{t}_2 = \vec{u}_y. \\ \vec{n} = \vec{t}_1 \times \vec{t}_2 = \frac{-a'_x \vec{u}_x + \vec{u}_z}{\sqrt{1 + a'^2_x}}, \end{cases} \quad (4)$$

where $a'_x = (\partial/\partial x)a_x$ is the partial derivative of the boundary profile in the x direction, and $\vec{u}_{x,y,z}$ are the unit vectors in the x, y and z directions. We use those tangential and normal vectors when considering the field continuity conditions or surface integrations over the modulated interface.

A. Fourier expansion of fields

Since the upper and lower spaces of the boundary are homogeneous dielectrics, we can unambiguously expand the incident, reflected and transmitted fields in a series

of plane waves,

$$\begin{cases} \vec{\mathcal{E}}_{\mathbf{x},z}^{\text{inc}} = \int_{\mathbf{k}} e^{i\mathbf{k}\cdot\mathbf{x}} \vec{E}_{\mathbf{k},z}^{->}, & \vec{\mathcal{H}}_{\mathbf{x},z}^{\text{inc}} = \int_{\mathbf{k}} e^{i\mathbf{k}\cdot\mathbf{x}} \vec{H}_{\mathbf{k},z}^{->}, \\ \vec{\mathcal{E}}_{\mathbf{x},z}^{\text{ref}} = \int_{\mathbf{k}} e^{i\mathbf{k}\cdot\mathbf{x}} \vec{E}_{\mathbf{k},z}^{+>}, & \vec{\mathcal{H}}_{\mathbf{x},z}^{\text{ref}} = \int_{\mathbf{k}} e^{i\mathbf{k}\cdot\mathbf{x}} \vec{H}_{\mathbf{k},z}^{+>}, \\ \vec{\mathcal{E}}_{\mathbf{x},z}^{\text{tra}} = \int_{\mathbf{k}} e^{i\mathbf{k}\cdot\mathbf{x}} \vec{E}_{\mathbf{k},z}^{-<}, & \vec{\mathcal{H}}_{\mathbf{x},z}^{\text{tra}} = \int_{\mathbf{k}} e^{i\mathbf{k}\cdot\mathbf{x}} \vec{H}_{\mathbf{k},z}^{-<}. \end{cases} \quad (5)$$

The superscripts on the left hand side ($\Lambda = \text{inc, ref, tra}$) are labels which identify modes in the real space and the time domain. The two superscripts on the right hand side ($\sigma = \pm, \tau = \gtrless$) are corresponding labels in the reciprocal space. While σ specifies in which direction the mode propagates, τ specifies in which medium the mode lives. The fields in the real space, $\vec{\mathcal{E}}_{\mathbf{x},z}$ and $\vec{\mathcal{H}}_{\mathbf{x},z}$, are given by means of complex-valued Fourier components, $\vec{E}_{\mathbf{k},z}$ and $\vec{H}_{\mathbf{k},z}$. Note that we have introduced a reciprocal vector $\mathbf{k} = \{k_x, k_y, -ik_0 = -i\omega/c\}$. Each Fourier component satisfies

$$\vec{E}_{\mathbf{k},z}^{\sigma\tau} = \vec{E}_{-\mathbf{k},z}^{\sigma\tau*}, \quad \vec{H}_{\mathbf{k},z}^{\sigma\tau} = \vec{H}_{-\mathbf{k},z}^{\sigma\tau*}. \quad (6)$$

These conditions are required because $\vec{\mathcal{E}}_{\mathbf{x},z}^{\sigma\tau}$ and $\vec{\mathcal{H}}_{\mathbf{x},z}^{\sigma\tau}$ are real-valued. We employ a shorthand notation for an integral operation,

$$\int_{\mathbf{k}} = \iint_{-\infty}^{+\infty} \frac{dk_x dk_y}{(2\pi)^2} \int_{-\infty}^{+\infty} \frac{d\omega}{2\pi}. \quad (7)$$

We substitute Eq. (5) into Maxwell's equations to get the Helmholtz equation,

$$\left[-\frac{\partial^2}{\partial z^2} - (\epsilon^\tau k_0^2 - k_{\parallel}^2) \right] \vec{E}_{\mathbf{k},z}^{\sigma\tau} = 0, \quad (8)$$

where we have defined $k_{\parallel} = \sqrt{k_x^2 + k_y^2}$. This differential equation can be easily solved,

$$\vec{E}_{\mathbf{k},z}^{\sigma\tau} = e^{i\sigma K_{\mathbf{k}}^\tau z} \vec{E}_{\mathbf{k},0}^{\sigma\tau}. \quad (9)$$

Here, $\vec{E}_{\mathbf{k},0}^{\sigma\tau}$ is a complex-valued vector at $z = 0$, which determines the amplitude and the polarisation, and we define the wavenumber in the z direction,

$$K_{\mathbf{k}}^\tau = \text{sgn}(\omega) \text{Re} \sqrt{\epsilon^\tau k_0^2 - k_{\parallel}^2} + i \text{Im} \sqrt{\epsilon^\tau k_0^2 - k_{\parallel}^2}. \quad (10)$$

We have added the prefactor $\text{sgn}(\omega)$ at the real part in order to take into account that the propagation direction of a wave reverses when the sign of the frequency is flipped [27]. Remind that the wavenumber satisfies $K_{-\mathbf{k}}^{\tau*} = -K_{\mathbf{k}}^\tau$.

In our dielectric medium, the field is divergenceless (i.e. $\nabla \cdot \vec{\mathcal{E}}_{\mathbf{x},z}^\Lambda = 0$) so that we have a transversality condition,

$$i(k_x \vec{u}_x + k_y \vec{u}_y + \sigma K_{\mathbf{k}}^\tau \vec{u}_z) \cdot \vec{E}_{\mathbf{k},0}^{\sigma\tau} = 0. \quad (11)$$

Following the same procedure, we can write the boundary matching equations in the y direction,

$$\vec{t}_2 \cdot (\vec{\mathcal{E}}_{\mathbf{x},a_{\mathbf{x}}}^{\text{inc}} + \vec{\mathcal{E}}_{\mathbf{x},a_{\mathbf{x}}}^{\text{ref}} - \vec{\mathcal{E}}_{\mathbf{x},a_{\mathbf{x}}}^{\text{tra}}) = 0, \quad (24)$$

$$\vec{t}_2 \cdot (\vec{\mathcal{H}}_{\mathbf{x},a_{\mathbf{x}}}^{\text{inc}} + \vec{\mathcal{H}}_{\mathbf{x},a_{\mathbf{x}}}^{\text{ref}} - \vec{\mathcal{H}}_{\mathbf{x},a_{\mathbf{x}}}^{\text{tra}}) = -\frac{\dot{a}_{\mathbf{x}}}{c} \alpha \eta \vec{t}_1 \cdot \frac{\vec{\mathcal{E}}_{\mathbf{x},a_{\mathbf{x}}}^{\text{tra}}}{Z_0}. \quad (25)$$

Since our modulation is invariant with respect to the translation in the y direction, the problem can be regarded as a two-dimensional one. Here, we investigate two fundamental cases where the incident field is either s - or p -polarised.

There is no polarisation rotation as we stick to the in-plane calculation. This is because our ‘optical axis’ induced by the surface structure of grating type is in the y direction, which is parallel or perpendicular to the electric and magnetic fields. In the s polarisation case, the electric field oscillates perpendicularly to the xz plane while the magnetic field oscillates in the xz plane. Therefore, Eqs. (20, 25) are automatically satisfied in the s polarisation case, and we can focus on

$$\begin{cases} \vec{t}_2 \cdot (\vec{\mathcal{E}}_{\mathbf{x},a_{\mathbf{x}}}^{\text{inc}} + \vec{\mathcal{E}}_{\mathbf{x},a_{\mathbf{x}}}^{\text{ref}} - \vec{\mathcal{E}}_{\mathbf{x},a_{\mathbf{x}}}^{\text{tra}}) = 0, \\ \eta \vec{t}_1 \cdot Z_0 (\vec{\mathcal{H}}_{\mathbf{x},a_{\mathbf{x}}}^{\text{inc}} + \vec{\mathcal{H}}_{\mathbf{x},a_{\mathbf{x}}}^{\text{ref}} - \vec{\mathcal{H}}_{\mathbf{x},a_{\mathbf{x}}}^{\text{tra}}) = \frac{\dot{a}_{\mathbf{x}}}{c} \alpha \vec{t}_2 \cdot \vec{\mathcal{E}}_{\mathbf{x},a_{\mathbf{x}}}^{\text{tra}}. \end{cases} \quad (26)$$

On the other hand, the magnetic field oscillates in the y direction in the p polarisation case, and the electric field lies in the xz plane. Thus, we can focus on

$$\begin{cases} \eta \vec{t}_1 \cdot (\vec{\mathcal{E}}_{\mathbf{x},a_{\mathbf{x}}}^{\text{inc}} + \vec{\mathcal{E}}_{\mathbf{x},a_{\mathbf{x}}}^{\text{ref}} - \vec{\mathcal{E}}_{\mathbf{x},a_{\mathbf{x}}}^{\text{tra}}) = 0, \\ \vec{t}_2 \cdot Z_0 (\vec{\mathcal{H}}_{\mathbf{x},a_{\mathbf{x}}}^{\text{inc}} + \vec{\mathcal{H}}_{\mathbf{x},a_{\mathbf{x}}}^{\text{ref}} - \vec{\mathcal{H}}_{\mathbf{x},a_{\mathbf{x}}}^{\text{tra}}) = -\frac{\dot{a}_{\mathbf{x}}}{c} \alpha \eta \vec{t}_1 \cdot \vec{\mathcal{E}}_{\mathbf{x},a_{\mathbf{x}}}^{\text{tra}}. \end{cases} \quad (27)$$

These simultaneous equations depend on space and time. Thanks to the time derivative of the surface profile $\dot{a}_{\mathbf{x}}$ and the tangential vector $\eta \vec{t}_1$ in Eqs. (26, 27), we can properly take both temporal and spatial modulations into consideration.

We apply the Fourier transform $\mathcal{F}[g_{\mathbf{x}}]_{\mathbf{k}} \equiv \int g_{\mathbf{x}} e^{-i\mathbf{k} \cdot \mathbf{x}} d\mathbf{x}$ to Eqs. (26, 27) to obtain equation systems determining the reflection and transmission matrices in the frequency domain.

Let take the s polarisation as an example. We use the Fourier expansion of the electric field (5, 15) to get

$$\vec{t}_2 \cdot \vec{\mathcal{E}}_{\mathbf{x},a_{\mathbf{x}}}^{\Lambda} = - \int_{\mathbf{k}} e^{i\mathbf{k} \cdot \mathbf{x}} \text{sgn}(\omega) \frac{k_x}{k_{\parallel}} e^{i\phi_{\mathbf{k}}^{\sigma\tau} \sin \mathbf{q} \cdot \mathbf{x}} E_{s,\mathbf{k}}^{\sigma\tau}, \quad (28)$$

where we have defined the propagating phase factor $\phi_{\mathbf{k}}^{\sigma\tau} = \sigma K_{\mathbf{k}}^{\tau} A$. We use the Jacobi-Anger identity to expand the exponential of the trigonometric function [28],

$$\vec{t}_2 \cdot \vec{\mathcal{E}}_{\mathbf{x},a_{\mathbf{x}}}^{\Lambda} = - \sum_{m,\mathbf{k}} e^{i\mathbf{k} \cdot \mathbf{x}} \frac{k_{x,m}}{k_{\parallel,m}} \text{sgn}(\omega_m) J_{-m}(\phi_{\mathbf{k}_m}^{\sigma\tau}) E_{s,\mathbf{k}_m}^{\sigma\tau}, \quad (29)$$

where J_m is the m^{th} order Bessel function of the first kind. Note that the integration variables are relevantly shifted, $\mathbf{k} \mapsto \mathbf{k}_m = \mathbf{k} + m\mathbf{q}$, after the expansion. Note also that we have introduced a shorthand notation,

$$\sum_{m,\mathbf{k}} = \sum_{m=-\infty}^{+\infty} \int_{\mathbf{k}}. \quad (30)$$

Applying the Fourier transform, we can obtain the l th order quantity,

$$\mathcal{F} \left[\vec{t}_2 \cdot \vec{\mathcal{E}}_{\mathbf{x},a_{\mathbf{x}}}^{\Lambda} \right]_{\mathbf{k}_l} = [\mathbf{M}_{\mathbf{k}}^{\sigma\tau} \mathbb{E}_{s,\mathbf{k}}^{\sigma\tau}]_l. \quad (31)$$

Here, we have collected the modal amplitude in each diffraction order into one column,

$$\mathbb{E}_{\lambda,\mathbf{k}}^{\sigma\tau} = \begin{pmatrix} \vdots \\ E_{\lambda,\mathbf{k}_{-1}}^{\sigma\tau} \\ E_{\lambda,\mathbf{k}_0}^{\sigma\tau} \\ E_{\lambda,\mathbf{k}_{+1}}^{\sigma\tau} \\ \vdots \end{pmatrix}, \quad (32)$$

and introduced a matrix-vector representation with the coefficient matrix that has the geometric information of the boundary,

$$[\mathbf{M}_{\mathbf{k}}^{\sigma\tau}]_{lm} = \frac{k_{x,m}}{k_{\parallel,m}} \text{sgn}(\omega_m) J_{l-m}(\phi_{\mathbf{k}_m}^{\sigma\tau}). \quad (33)$$

Here, the Bessel function is responsible for the correlation between the l th order and the m th order diffraction. The diffraction is stronger as the surface corrugation depth increases with respect to the wavenumber in the z direction. This is why we provide $\phi_{\mathbf{k}_m}^{\sigma\tau} = \sigma K_{\mathbf{k}_m}^{\sigma\tau} A$ in the argument.

Finally, applying the Fourier transform to Eq. (24), we can obtain

$$\mathbf{M}_{\mathbf{k}}^{->} \mathbb{E}_{s,\mathbf{k}}^{->} + \mathbf{M}_{\mathbf{k}}^{+>} \mathbb{E}_{s,\mathbf{k}}^{+>} - \mathbf{M}_{\mathbf{k}}^{-<} \mathbb{E}_{s,\mathbf{k}}^{-<} = 0. \quad (34)$$

Similarly, we can perform the Fourier transform for the boundary condition of the magnetic field. The tangential component of the magnetic field is evaluated as below:

$$\eta \vec{t}_1 \cdot Z_0 \vec{\mathcal{H}}_{\mathbf{x},a_{\mathbf{x}}}^{\Lambda} = \int_{\mathbf{k}} e^{i\mathbf{k} \cdot \mathbf{x}} e^{i\sigma K_{\mathbf{k}}^{\tau} a_{\mathbf{x}}} \eta \vec{t}_1 \cdot \vec{h}_{s,\mathbf{k}}^{\sigma\tau} Z_0 H_{s,\mathbf{k}}^{\sigma\tau}, \quad (35)$$

$$= \int_{\mathbf{k}} e^{i\mathbf{k} \cdot \mathbf{x}} \frac{\sigma K_{\mathbf{k}}^{\tau} k_x - a'_{\mathbf{x}} k_{\parallel}^2}{k_{\parallel} |k_0|} e^{i\sigma K_{\mathbf{k}}^{\tau} a_{\mathbf{x}}} E_{s,\mathbf{k}}^{\sigma\tau}, \quad (36)$$

$$= \sum_{m,\mathbf{k}} e^{i(\mathbf{k}-m\mathbf{q}) \cdot \mathbf{x}} \left(\frac{k_x}{k_{\parallel}} \frac{\sigma K_{\mathbf{k}}^{\tau}}{|k_0|} - \frac{-mg}{\sigma K_{\mathbf{k}}^{\tau} |k_0|} \right) J_{-m}(\phi_{\mathbf{k}}^{\sigma\tau}) E_{s,\mathbf{k}}^{\sigma\tau}, \quad (37)$$

where we expanded the exponential of the trigonometric function by using the Bessel functions. Applying the Fourier transform to Eq. (23) gives

$$\mathbf{N}_{\mathbf{k}}^{->} \mathbb{E}_{s,\mathbf{k}}^{->} + \mathbf{N}_{\mathbf{k}}^{+>} \mathbb{E}_{s,\mathbf{k}}^{+>} - (\mathbf{N}_{\mathbf{k}}^{-<} + \mathbf{L}_{\mathbf{k}}) \mathbb{E}_{s,\mathbf{k}}^{-<} = 0. \quad (38)$$

Here, the element of the coefficient matrix is given by

$$[\mathbf{L}_{\mathbf{k}}]_{lm} = \frac{\alpha}{c} \frac{(l-m)\Omega}{-K_{\mathbf{k}_m}^<} \times \text{sgn}(\omega_m) \frac{k_{x,m}}{k_{\parallel,m}} J_{l-m}(\phi_{\mathbf{k}_m}^{<-}), \quad (39)$$

$$[\mathbf{N}_{\mathbf{k}}^{\sigma\tau}]_{lm} = \left(\frac{k_{x,m}}{k_{\parallel,m}} \frac{\sigma K_{\mathbf{k}_m}^{\sigma\tau}}{|k_{0,m}|} - \frac{(l-m)g}{\sigma K_{\mathbf{k}_m}^{\sigma\tau}} \frac{k_{\parallel,m}}{|k_{0,m}|} \right) J_{l-m}(\phi_{\mathbf{k}_m}^{\sigma\tau}). \quad (40)$$

The expressions of \mathbf{L} and \mathbf{N} are relatively intricate, compared with the \mathbf{M} matrix. The \mathbf{L} matrix is responsible for the induced surface current (22), and thus its matrix elements are proportional to the permittivity difference α . The factor of $[(l-m)\Omega]/(-K_{\mathbf{k}_m}^<)$ is produced by the time derivative $\dot{\mathbf{a}}_{\mathbf{x}}$ that we have in the expression of the surface current (22). As for the \mathbf{N} matrix, the non-uniform vectorial line element, $\eta \vec{t}_1 = \vec{u}_x + a'_x \vec{u}_z$, makes the expression complicated. The first and second terms in Eq. (40) stems from the field matching in the x and z directions, respectively. The space derivative a'_x yields the factor of $[(l-m)g]/(\sigma K_{\mathbf{k}_m}^{\sigma\tau})$ in the second term. It is worth noting that here we can define the incident angle θ_{in} by

$$\cos \theta_{\text{in}} = \frac{\sigma K_{\mathbf{k}}^>}{|k_0|}, \quad \sin \theta_{\text{in}} = \frac{k_{\parallel}}{|k_0|}. \quad (41)$$

Here, we observe that the \mathbf{M} , \mathbf{N} and \mathbf{L} matrices does not change if we keep the ratio between any two lengths and just scale the parameters. All of the matrix elements are given by means of dimensionless numbers such as $K_{\mathbf{k}}^<A$ and $g/K_{\mathbf{k}}^<$.

Those quantities are invariant under the scaling of the modulation depth A and the reciprocal vectors, \mathbf{q} and \mathbf{k} ,

$$\begin{cases} A \mapsto \beta A, & \mathbf{q} \mapsto \beta^{-1} \mathbf{q}, \\ \mathbf{k} \mapsto \beta^{-1} \mathbf{k}, \end{cases} \quad (42)$$

where β is the scale factor. Since the effects of the spatiotemporal modulation is encoded by the \mathbf{M} , \mathbf{N} and \mathbf{L} matrices, the scaling does not affect the calculation.

Let us rearrange Eqs. (34, 38) in a matrix form,

$$\begin{pmatrix} \mathbf{M}_{\mathbf{k}}^{+>} & -\mathbf{M}_{\mathbf{k}}^{-<} \\ \mathbf{N}_{\mathbf{k}}^{+>} & -(\mathbf{N}_{\mathbf{k}}^{-<} + \mathbf{L}_{\mathbf{k}}) \end{pmatrix} \begin{pmatrix} \mathbb{E}_{s,\mathbf{k}}^{+>} \\ \mathbb{E}_{s,\mathbf{k}}^{-<} \end{pmatrix} = \begin{pmatrix} -\mathbf{M}_{\mathbf{k}}^{->} \mathbb{E}_{s,\mathbf{k}}^{->} \\ -\mathbf{N}_{\mathbf{k}}^{->} \mathbb{E}_{s,\mathbf{k}}^{->} \end{pmatrix}. \quad (43)$$

This is the scattering equation for the s polarisation incidence.

By following the same procedure, we can obtain the matrix equation for the p polarisation,

$$\begin{pmatrix} \mathbf{M}_{\mathbf{k}}^{+>} & -(\mathbf{M}_{\mathbf{k}}^{-<} + \tilde{\mathbf{L}}_{\mathbf{k}}) \\ \tilde{\mathbf{N}}_{\mathbf{k}}^{+>} & -\tilde{\mathbf{N}}_{\mathbf{k}}^{-<} \end{pmatrix} \begin{pmatrix} \mathbb{H}_{p,\mathbf{k}}^{+>} \\ \mathbb{H}_{p,\mathbf{k}}^{-<} \end{pmatrix} = \begin{pmatrix} -\mathbf{M}_{\mathbf{k}}^{->} \mathbb{H}_{p,\mathbf{k}}^{->} \\ -\tilde{\mathbf{N}}_{\mathbf{k}}^{->} \mathbb{H}_{p,\mathbf{k}}^{->} \end{pmatrix}, \quad (44)$$

where we have defined $\tilde{\mathbf{N}}_{\mathbf{k}}^{\sigma\tau} = \mathbf{N}_{\mathbf{k}}^{\sigma\tau}/\epsilon^{\tau}$. Note that the electric current contribution $\tilde{\mathbf{L}}$ appears not with the $\tilde{\mathbf{N}}$ matrix but with the $\tilde{\mathbf{M}}$ matrix. Please see the Appendix A for the derivation.

III. NUMERICAL IMPLEMENTATION

Inverting Eqs. (43, 44), we can get the reflection and transmission matrices,

$$\begin{pmatrix} \mathbf{R}_{s,\mathbf{k}} \\ \mathbf{T}_{s,\mathbf{k}} \end{pmatrix} = \begin{pmatrix} \mathbf{M}_{\mathbf{k}}^{+>} & -\mathbf{M}_{\mathbf{k}}^{-<} \\ \mathbf{N}_{\mathbf{k}}^{+>} & -(\mathbf{N}_{\mathbf{k}}^{-<} + \mathbf{L}_{\mathbf{k}}) \end{pmatrix}^{-1} \begin{pmatrix} -\mathbf{M}_{\mathbf{k}}^{->} \\ -\mathbf{N}_{\mathbf{k}}^{->} \end{pmatrix}, \quad (45)$$

$$\begin{pmatrix} \mathbf{R}_{p,\mathbf{k}} \\ \mathbf{T}_{p,\mathbf{k}} \end{pmatrix} = \begin{pmatrix} \mathbf{M}_{\mathbf{k}}^{+>} & -(\mathbf{M}_{\mathbf{k}}^{-<} + \tilde{\mathbf{L}}_{\mathbf{k}}) \\ \tilde{\mathbf{N}}_{\mathbf{k}}^{+>} & -\tilde{\mathbf{N}}_{\mathbf{k}}^{-<} \end{pmatrix}^{-1} \begin{pmatrix} -\mathbf{M}_{\mathbf{k}}^{->} \\ -\mathbf{N}_{\mathbf{k}}^{->} \end{pmatrix}. \quad (46)$$

Note that only the diagonal elements of $\mathbf{M}_{\mathbf{k}}^{\sigma\tau}$ and $\mathbf{N}_{\mathbf{k}}^{\sigma\tau}$ remain finite in the flat boundary limit ($A \rightarrow 0$), and all other matrix elements vanish so that Eqs. (45, 46) recover the Fresnel coefficients (See the Appendix B).

When we numerically evaluate the reflection and transmission matrices, we truncate the \mathbf{M} , \mathbf{N} and \mathbf{L} matrices to finite rank ones so that $-m_c \leq l \leq +m_c$ and $-m_c \leq m \leq +m_c$, where m_c is the cutoff number. Since our boundary is differentiable and the media above and below the boundary are homogeneous, the truncation can be justified as in the conventional Fourier modal methods [29, 30]. As shown in FIG. 3, we can also numerically confirm that large matrix elements are highly localised near the diagonal elements.

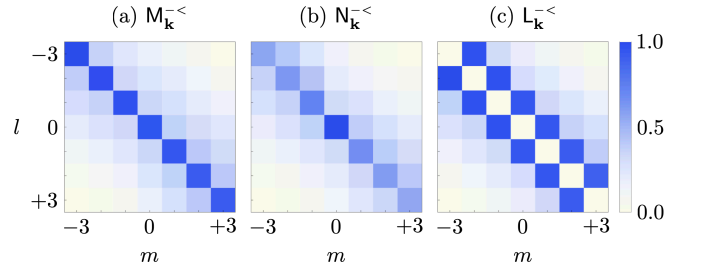


FIG. 3. Typical distribution of the matrix elements. The absolute values of the matrix elements in \mathbf{M} , \mathbf{N} and \mathbf{L} are plotted. The common colorbar is shown on the right of (c). The horizontal and vertical axes are the column and row indices. Note that all elements are normalised by the maximum element in each matrix. In these plots, we use the following parameters: $\epsilon^> = 1.0$, $\epsilon^< = 2.25$, $A = 10$ [nm], $g = 2\pi$ [μm^{-1}], $\Omega = 0.2gc$, $\omega_{\text{in}} = 0.8gc$, $\theta_{\text{in}} = 0$, $k_y = 0$. The cutoff number is $m_c = 3$.

When the modulation strength is sufficiently weak compared with the spatial and temporal modulation period ($gA \ll 1$, and $\Omega A/c \ll 1$), the surface structure is homogenised from the perspective of the electromagnetic field. In other words, the field is slowly varying near the grating, and thus we can consider effective infinitesimally thin medium to model the deformed boundary. The effective medium is given by means of permittivity averaging in the z direction,

$$\epsilon_{\mathbf{x}}^{\text{sf}} = \int_{-A}^{+A} dz \epsilon_{\mathbf{x},z} = \bar{\epsilon}(1 + 2i\kappa \sin \mathbf{q} \cdot \mathbf{x}) \quad (47)$$

where we have defined effective parameters,

$$\bar{\epsilon} = (\epsilon^< + \epsilon^>)A, \quad \kappa = \frac{1}{2i} \frac{\epsilon^< - \epsilon^>}{\epsilon^< + \epsilon^>}. \quad (48)$$

With the permittivity averaging procedure, we can get a very thin grating as the effective thin medium (see FIG. 4). The scattering calculation within the effective

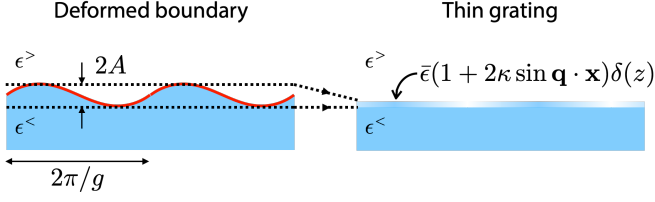


FIG. 4. Homogenisation. Averaging the permittivity in the z direction within the modulated region ($-A \leq z \leq +A$) generates a very thin grating model.

medium description is shown in the Supplemental Materials [31].

In FIG. 5, we compare the incident angle dependences of the first order diffraction amplitudes calculated within the dynamical differential formalism and that within the homogenisation theory. We can clearly recognise that the angular spectra calculated in two different method agree well. Under the flipping both of the sign of diffraction orders and the incident angle, the graph is symmetric if there is no time dependence ($\Omega = 0$). This is a consequence of the discrete translational invariance of the system. If we introduce the temporal modulation ($\Omega \neq 0$), the system is no longer invariant the translation and non-reciprocal. This is why the plots are asymmetric when $\Omega \neq 0$.

In FIG. 6, we compare the first order diffraction amplitudes spectra generated by the dynamical differential formalism and the homogenisation approach. We can see that the two approaches agree well. If there is no temporal modulation ($\Omega = 0$), the positive and negative diffraction spectra are the same. This recovers the fact that diffraction at the static grating is symmetric. Once the temporal modulation is introduced ($\Omega \neq 0$), the positive and negative spectra start to deviate from each other. Again, this implies that the spatiotemporal modulation breaks the reciprocity of our system.

In FIG. 7, we compare the modulation strength dependences of the first order diffraction amplitudes. It is clear that two approaches agree when the modulation strength is small. Both positive and negative diffraction intensities have quadratic dependence.

IV. CONCLUSIONS

In this study, we proposed a dynamical differential formalism which enables analytical calculation of the scattering by a surface modulated both in space and time. Using dynamical coordinate transformation generated by the boundary profile, we can directly impose the boundary conditions at the dynamically deformed interface for both electric and magnetic fields to properly capture the geometry and motion. In the numerical calculation, we

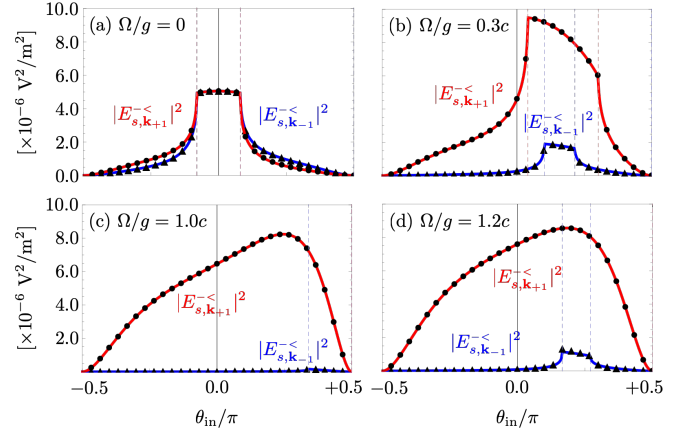


FIG. 5. Incident angle dependences of the first order diffraction intensities. The horizontal axes are the incident angle defined by Eq. (41). The blue (red) curve corresponds to the negative (positive) diffraction $|E_{s,k_{-1}}^{-<}|^2$ ($|E_{s,k_{+1}}^{<-}|^2$) inside the dielectric medium calculated by the dynamical differential formalism. The black circles and triangles are generated by the effective medium description. At dashed lines corresponding to the emergence of diffraction modes ($K_{\pm 1}^{\tau} = 0$), the angular spectra are singular, that is a Wood grating anomaly [32]. In these figures, we substitute the following parameters: $\epsilon^+ = 1.0$, $\epsilon^- = 2.25$, $g = 2\pi [\mu\text{m}^{-1}]$, $A = 1 [\text{nm}]$, $\lambda = s$, $\omega_{\text{in}} = 0.8gc$, $k_y = 0$. The cutoff number is $m_c = 3$.

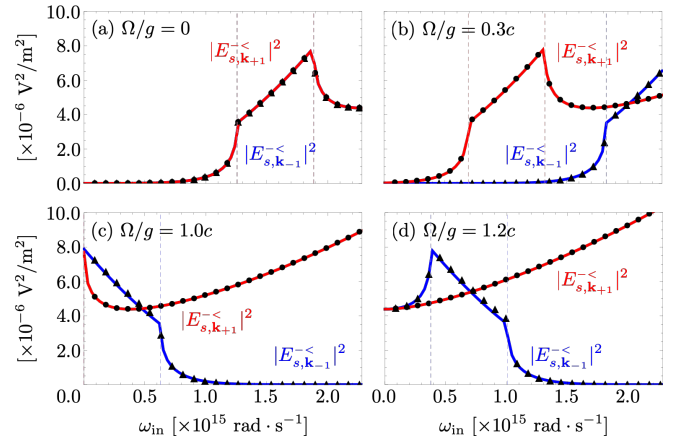


FIG. 6. Frequency spectra of the first order diffraction amplitudes. The blue (red) curve corresponds to the negative (positive) diffraction amplitude $|E_{s,k_{-1}}^{-<}|^2$ ($|E_{s,k_{+1}}^{<-}|^2$) calculated by the dynamical differential formalism. Note that red and blue curves are completely overlap one another in (a). In these plots, we use the following parameters: $\epsilon^+ = 1.0$, $\epsilon^- = 2.25$, $g = 2\pi [\mu\text{m}^{-1}]$, $A = 1 [\text{nm}]$, $\lambda = s$, $\theta_{\text{in}} = 0$, $k_y = 0$. The cutoff number is $m_c = 3$.

confirmed our formalism is consistent with the effective medium description. The diffraction spectra of the surface become asymmetric in the presence temporal modulation.

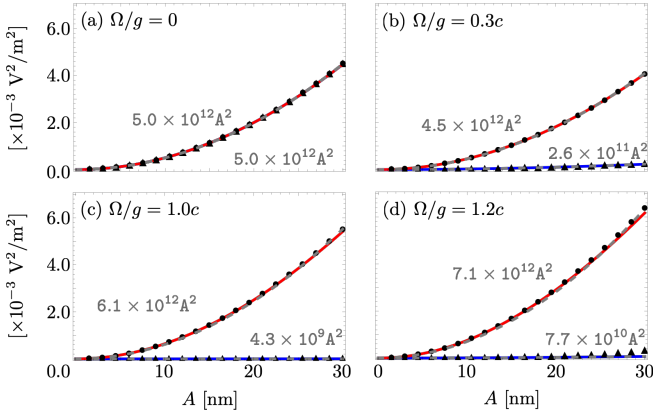


FIG. 7. Modulation strength dependence of the first order diffraction intensities. The blue (red) curve corresponds to the negative (positive) diffraction $|E_{s,\mathbf{k}-1}^{-<}|^2$ ($|E_{s,\mathbf{k}+1}^{-<}|^2$) inside the dielectric medium calculated by the dynamical differential formalism. The black circles and triangles are produced by the effective medium approach. Both positive and negative intensities quadratically depend on the modulation strength as the data is fitted by parabolic curves (grey dashed curves). The fitting equations are shown in each figure. Note that positive and negative diffraction intensities are completely overlap one another in (a). In these plots, we use the following parameters: $\epsilon^> = 1.0$, $\epsilon^< = 2.25$, $g = 2\pi [\mu\text{m}^{-1}]$, $\omega_{\text{in}} = 0.8gc$, $\theta_{\text{in}} = 0$, $k_y = 0$. The cutoff number is $m_c = 3$.

ACKNOWLEDGMENTS

D.O. is funded by the President's PhD Scholarships at Imperial College London. K.D. and J.B.P. acknowledges support from the Gordon and Betty Moore Foundation.

Appendix A: p polarisation case

In the p polarisation case, the tangential component of the electric field is

$$\eta \vec{t}_1 \cdot \vec{\mathcal{E}}_{\mathbf{x},a\mathbf{x}}^\Lambda = \int_{\mathbf{k}} e^{i\mathbf{k} \cdot \mathbf{x}} e^{i\sigma K_{\mathbf{k}}^\tau a\mathbf{x}} Z_{p,\mathbf{k}}^\tau H_{p,\mathbf{k}}^{\sigma\tau} \eta \vec{t}_1 \cdot \vec{e}_{p,\mathbf{k}}^{\sigma\tau} \quad (\text{A1})$$

$$= \int_{\mathbf{k}} e^{i\mathbf{k} \cdot \mathbf{x}} \frac{Z_0}{\epsilon^\tau} e^{i\sigma K_{\mathbf{k}}^\tau a\mathbf{x}} \frac{\sigma K_{\mathbf{k}}^\tau k_x - a'_{\mathbf{x}} k_{\parallel}^2}{k_{\parallel} |k_0|} H_{p,\mathbf{k}}^{\sigma\tau}, \quad (\text{A2})$$

where we have used the fact that the electric and magnetic amplitude can be associated with each other,

$$\begin{cases} E_{s,\mathbf{k}}^{\sigma\tau} = Z_{s,\mathbf{k}}^\tau H_{s,\mathbf{k}}^{\sigma\tau}, \\ E_{p,\mathbf{k}}^{\sigma\tau} = Z_{p,\mathbf{k}}^\tau H_{p,\mathbf{k}}^{\sigma\tau}, \end{cases} \quad (\text{A3})$$

via the characteristic impedance,

$$Z_{\lambda,\mathbf{k}}^\tau = \begin{cases} \frac{Z_0}{\sqrt{\epsilon^\tau}} \sqrt{\frac{\omega^2 \epsilon^\tau / c^2}{|K_{\mathbf{k}}^\tau|^2 + k_{\parallel}^2}} & (\lambda = s), \\ \frac{Z_0}{\sqrt{\epsilon^\tau}} \sqrt{\frac{|K_{\mathbf{k}}^\tau|^2 + k_{\parallel}^2}{\omega^2 \epsilon^\tau / c^2}} & (\lambda = p), \end{cases} \quad (\text{A4})$$

where $Z_0 = \sqrt{\mu_0/\epsilon_0}$ is the impedance of free space. We use the Jacobi-Anger identity and perform the Fourier transform,

$$\mathcal{F} \left[\eta \vec{t}_1 \cdot \vec{\mathcal{E}}_{\mathbf{x},z}^\Lambda \right]_{\mathbf{k}_l} = Z_0 \left[\tilde{\mathbf{N}}_{\mathbf{k}}^{\sigma\tau} \mathbb{H}_{p,\mathbf{k}}^{\sigma\tau} \right]_l, \quad (\text{A5})$$

where we have defined $\tilde{\mathbf{N}}_{\mathbf{k}}^{\sigma\tau} = \mathbf{N}_{\mathbf{k}}^{\sigma\tau} / \epsilon^\tau$. Applying the Fourier transform to Eq. (20) gives

$$\tilde{\mathbf{N}}_{\mathbf{k}}^{->} \mathbb{H}_{p,\mathbf{k}}^{->} + \tilde{\mathbf{N}}_{\mathbf{k}}^{+>} \mathbb{H}_{p,\mathbf{k}}^{+>} - \tilde{\mathbf{N}}_{\mathbf{k}}^{-<} \mathbb{H}_{p,\mathbf{k}}^{-<} = 0. \quad (\text{A6})$$

Note that we have divide the equation by the impedance of free space Z_0 to make the coefficient matrix dimensionless.

Next, we evaluate the tangential component of the magnetic field,

$$\vec{t}_2 \cdot \vec{\mathcal{H}}_{\mathbf{x},a\mathbf{x}}^\Lambda = - \int_{\mathbf{k}} e^{i\mathbf{k} \cdot \mathbf{x}} \text{sgn}(\omega) \frac{k_x}{k_{\parallel}} e^{i\phi_{\mathbf{k}}^{\sigma\tau} \sin \mathbf{q} \cdot \mathbf{x}} H_{p,\mathbf{k}}^{\sigma\tau}. \quad (\text{A7})$$

Using the Jacobi-Anger identity and applying the Fourier transform, we can obtain the l th order quantity,

$$\mathcal{F} \left[\vec{t}_2 \cdot \vec{\mathcal{H}}_{\mathbf{x},a\mathbf{x}}^\Lambda \right]_{\mathbf{k}_l} = [\mathbf{M}_{\mathbf{k}}^{\sigma\tau} \mathbb{H}_{p,\mathbf{k}}^{\sigma\tau}]_l, \quad (\text{A8})$$

where the \mathbf{M} matrix is given in Eq. (33).

The surface current contribution is evaluated as

$$\mathcal{F} \left[-\frac{\dot{a}_{\mathbf{x}}}{c} \alpha \eta \vec{t}_1 \cdot \frac{\vec{\mathcal{E}}_{\mathbf{x},a\mathbf{x}}^{\text{tra}}}{Z_0} \right]_{\mathbf{k}_l} = [\tilde{\mathbf{L}}_{\mathbf{k}} \mathbb{H}_{p,\mathbf{k}}^{-<}]_l \quad (\text{A9})$$

where we have introduced

$$\tilde{\mathbf{L}}_{\mathbf{k}} = \frac{A\Omega}{c} \alpha \left\{ [\mathbf{N}_{\mathbf{k}}^{-<}]_{l-1,m} + [\mathbf{N}_{\mathbf{k}}^{-<}]_{l+1,m} \right\}. \quad (\text{A10})$$

Substituting those result into the boundary matching equation (27), we can reach a matrix equation,

$$\mathbf{M}_{\mathbf{k}}^{->} \mathbb{H}_{p,\mathbf{k}}^{\text{inc}} + \mathbf{M}_{\mathbf{k}}^{+>} \mathbb{H}_{p,\mathbf{k}}^{\text{ref}} - (\mathbf{M}_{\mathbf{k}}^{-<} + \tilde{\mathbf{L}}_{\mathbf{k}}) \mathbb{H}_{p,\mathbf{k}}^{\text{tra}} = 0. \quad (\text{A11})$$

Finally, we can obtain the matrix equation which determine the reflection and transmission matrices,

$$\begin{pmatrix} \mathbf{M}_{\mathbf{k}}^{+>} & -\mathbf{M}_{\mathbf{k}}^{-<} \\ \tilde{\mathbf{N}}_{\mathbf{k}}^{+>} & -\tilde{\mathbf{N}}_{\mathbf{k}}^{-<} \end{pmatrix} \begin{pmatrix} \mathbb{H}_{p,\mathbf{k}}^{+>} \\ \mathbb{H}_{p,\mathbf{k}}^{-<} \end{pmatrix} = \begin{pmatrix} -\mathbf{M}_{\mathbf{k}}^{->} \mathbb{H}_{p,\mathbf{k}}^{->} \\ -\tilde{\mathbf{N}}_{\mathbf{k}}^{->} \mathbb{H}_{p,\mathbf{k}}^{->} \end{pmatrix}. \quad (\text{A12})$$

It is worth reminding that the characteristic impedance matrix,

$$\mathbf{Z}_{p,\mathbf{k}}^\tau = \text{diag}(\cdots, Z_{p,\mathbf{k}-1}^\tau, Z_{p,\mathbf{k}_0}^\tau, Z_{p,\mathbf{k}+1}^\tau, \cdots), \quad (\text{A12})$$

enables us to convert the reflection matrix calculated by means of the magnetic field,

$$\mathbb{H}_{p,\mathbf{k}}^{+>} = \mathbf{R}_{p,\mathbf{k}} \mathbb{H}_{p,\mathbf{k}}^{->}, \quad (\text{A13})$$

$$\mathbb{E}_{p,\mathbf{k}}^{+>} = \mathbf{Z}_{p,\mathbf{k}}^{>} \mathbf{R}_{p,\mathbf{k}} \mathbf{Z}_{p,\mathbf{k}}^{>-1} \mathbb{E}_{p,\mathbf{k}}^{->}, \quad (\text{A14})$$

and the transmission matrix,

$$\mathbb{H}_{p,\mathbf{k}}^{<-} = \mathbf{T}_{p,\mathbf{k}} \mathbb{H}_{p,\mathbf{k}}^{->}, \quad (\text{A15})$$

$$\mathbb{E}_{p,\mathbf{k}}^{<-} = \mathbf{Z}_{p,\mathbf{k}}^{<-} \mathbf{T}_{p,\mathbf{k}} \mathbf{Z}_{p,\mathbf{k}}^{<-1} \mathbb{E}_{p,\mathbf{k}}^{->}. \quad (\text{A16})$$

Appendix B: Recover the Fresnel equations

In the flat boundary limit ($A \rightarrow 0$), all the Bessel functions except the 0th order vanish,

$$\lim_{A \rightarrow 0} J_{l-m}(\phi_{\mathbf{k}_m}^{\sigma\tau}) = \delta_{l,m}, \quad (\text{B1})$$

and the matrices become diagonal

$$\begin{cases} [\mathbf{M}_{\mathbf{k}}^{\sigma\tau}]_{lm} & \rightarrow \frac{k_{x,m}}{k_{\parallel,m}} \text{sgn}(\omega_m) \delta_{l,m} \\ [\mathbf{N}_{\mathbf{k}}^{\sigma\tau}]_{lm} & \rightarrow \frac{k_{x,m}}{k_{\parallel,m}} \frac{\sigma K_{\mathbf{k},m}^{\tau}}{|k_{0,m}|} \delta_{l,m} \end{cases} \quad (A \rightarrow 0). \quad (\text{B2})$$

Therefore, the matrix equations (45, 46) are reduced and give the conventional Fresnel coefficients,

$$\begin{pmatrix} R_{s,\mathbf{k}} \\ T_{s,\mathbf{k}} \end{pmatrix} \rightarrow \begin{pmatrix} \frac{k_x}{k_{\parallel}} & -\frac{k_x}{k_{\parallel}} \\ \frac{k_x K_{\mathbf{k}}^{>}}{k_{\parallel} k_0} & \frac{k_x K_{\mathbf{k}}^{<}}{k_{\parallel} k_0} \end{pmatrix}^{-1} \begin{pmatrix} -\frac{k_x}{k_{\parallel}} \\ \frac{k_x K_{\mathbf{k}}^{>}}{k_{\parallel} k_0} \end{pmatrix} \quad (\text{B3})$$

$$= \begin{pmatrix} \frac{K_{\mathbf{k}}^{>} - K_{\mathbf{k}}^{<}}{K_{\mathbf{k}}^{>} + K_{\mathbf{k}}^{<}} \\ \frac{2K_{\mathbf{k}}^{>}}{K_{\mathbf{k}}^{>} + K_{\mathbf{k}}^{<}} \end{pmatrix}, \quad (\text{B4})$$

$$\begin{pmatrix} R_{p,\mathbf{k}} \\ T_{p,\mathbf{k}} \end{pmatrix} \rightarrow \begin{pmatrix} \frac{k_x}{k_{\parallel}} & -\frac{k_x}{k_{\parallel}} \\ \frac{k_x K_{\mathbf{k}}^{>}}{k_{\parallel} k_0 \epsilon^{>}} & \frac{k_x K_{\mathbf{k}}^{<}}{k_{\parallel} k_0 \epsilon^{<}} \end{pmatrix}^{-1} \begin{pmatrix} -\frac{k_x}{k_{\parallel}} \\ \frac{k_x K_{\mathbf{k}}^{>}}{k_{\parallel} k_0 \epsilon^{>}} \end{pmatrix} \quad (\text{B5})$$

$$= \begin{pmatrix} \frac{K_{\mathbf{k}}^{>}/\epsilon^{>} - K_{\mathbf{k}}^{<}/\epsilon^{<}}{K_{\mathbf{k}}^{>}/\epsilon^{>} + K_{\mathbf{k}}^{<}/\epsilon^{<}} \\ \frac{2K_{\mathbf{k}}^{>}/\epsilon^{>}}{K_{\mathbf{k}}^{>}/\epsilon^{>} + K_{\mathbf{k}}^{<}/\epsilon^{<}} \end{pmatrix}. \quad (\text{B6})$$

-
- [1] D. L. Sounas and A. Alù, Non-reciprocal photonics based on time modulation, *Nature Photonics* **11**, 774 (2017).
 - [2] C. Caloz, A. Alù, S. Tretyakov, D. Sounas, K. Achouri, and Z.-L. Deck-Léger, Electromagnetic nonreciprocity, *Physical Review Applied* **10**, 047001 (2018).
 - [3] A. M. Shaltout, V. M. Shalae, and M. L. Brongersma, Spatiotemporal light control with active metasurfaces, *Science* **364** (2019).
 - [4] E. Galiffi, P. Huidobro, and J. Pendry, Broadband nonreciprocal amplification in luminal metamaterials, *Physical Review Letters* **123**, 206101 (2019).
 - [5] P. A. Huidobro, E. Galiffi, S. Guenneau, R. V. Craster, and J. Pendry, Fresnel drag in space-time-modulated metamaterials, *Proceedings of the National Academy of Sciences* **116**, 24943 (2019).
 - [6] G. H. Goedecke and S. G. O'Brien, Scattering by irregular inhomogeneous particles via the digitized green's function algorithm, *Applied Optics* **27**, 2431 (1988).
 - [7] M. Yurkin and A. Hoekstra, The discrete dipole approximation: An overview and recent developments, *Journal of Quantitative Spectroscopy and Radiative Transfer* **106**, 558 (2007).
 - [8] G. Mie, Beiträge zur optik trüber medien, speziell kolloidaler metallösungen, *Annalen der physik* **330**, 377 (1908).
 - [9] J. Chandezon, G. Raoult, and D. Maystre, A new theoretical method for diffraction gratings and its numerical application, *Journal of Optics* **11**, 235 (1980).
 - [10] J. Chandezon, M. Dupuis, G. Cornet, and D. Maystre, Multicoated gratings: a differential formalism applicable in the entire optical region, *JOSA* **72**, 839 (1982).
 - [11] L. Li, Multilayer-coated diffraction gratings: differential method of chandezon et al. revisited, *JOSA A* **11**, 2816 (1994).
 - [12] L. Li and J. Chandezon, Improvement of the coordinate transformation method for surface-relief gratings with sharp edges, *JOSA A* **13**, 2247 (1996).
 - [13] L. Li, Use of fourier series in the analysis of discontinuous periodic structures, *JOSA A* **13**, 1870 (1996).
 - [14] W. Barnes, T. Preist, S. Kitson, J. Sambles, N. Cotter, and D. Nash, Photonic gaps in the dispersion of surface plasmons on gratings, *Physical Review B* **51**, 11164 (1995).
 - [15] J. Harris, T. Preist, and J. Sambles, Differential formalism for multilayer diffraction gratings made with uniaxial materials, *JOSA A* **12**, 1965 (1995).
 - [16] W. L. Barnes, T. Preist, S. Kitson, and J. Sambles, Physical origin of photonic energy gaps in the propagation of surface plasmons on gratings, *Physical Review B* **54**, 6227 (1996).
 - [17] J. Harris, T. Preist, E. Wood, and J. Sambles, Conical diffraction from multicoated gratings containing uniaxial materials, *JOSA A* **13**, 803 (1996).
 - [18] Y. Kitamura and S. Murakami, Hermitian two-band model for one-dimensional plasmonic crystals, *Physical Review B* **88**, 045406 (2013).

- [19] G. Murtaza, A. A. Syed, and Q. A. Naqvi, Study of scattering from a periodic grating structure using lorentz-drude model and chandezon method, *Optik* **133**, 9 (2017).
- [20] A. Ward and J. B. Pendry, Refraction and geometry in maxwell's equations, *Journal of modern optics* **43**, 773 (1996).
- [21] U. Leonhardt, Optical conformal mapping, *Science* **312**, 1777 (2006).
- [22] Y. Liu, T. Zentgraf, G. Bartal, and X. Zhang, Transformational plasmon optics, *Nano Letters* **10**, 1991 (2010).
- [23] A. Vakil and N. Engheta, Transformation optics using graphene, *Science* **332**, 1291 (2011).
- [24] L. Xu and H. Chen, Conformal transformation optics, *Nature Photonics* **9**, 15 (2015).
- [25] J. Pendry, Y. Luo, and R. Zhao, Transforming the optical landscape, *Science* **348**, 521 (2015).
- [26] J. Pendry, P. A. Huidobro, and K. Ding, Computing one-dimensional metasurfaces, *Physical Review B* **99**, 085408 (2019).
- [27] J. Pendry, Time reversal and negative refraction, *Science* **322**, 71 (2008).
- [28] A. A. Cuyt, V. Petersen, B. Verdonk, H. Waadeland, and W. B. Jones, *Handbook of continued fractions for special functions* (Springer Science & Business Media, 2008).
- [29] L. Li, Justification of matrix truncation in the modal methods of diffraction gratings, *Journal of Optics A: Pure and Applied Optics* **1**, 531 (1999).
- [30] A. A. Shcherbakov and A. V. Tishchenko, Efficient curvilinear coordinate method for grating diffraction simulation, *Optics express* **21**, 25236 (2013).
- [31] See the Supplemental Materials.
- [32] R. W. Wood, XLII. On a remarkable case of uneven distribution of light in a diffraction grating spectrum, *The London, Edinburgh, and Dublin Philosophical Magazine and Journal of Science* **4**, 396 (1902).